JOURNAL OF SOLID STATE CHEMISTRY **138,** 114–125 (1998)
ARTICLE NO. SC987761

Mechanochemical Synthesis of Fe–S Materials

J. Z. Jiang,*,[1] R. K. Larsen,* R. Lin,* S. Mørup,* I. Chorkendorff,* K. Nielsen,† K. Hansen,† and K. West†

*Department of Physics, Building 307, Technical University of Denmark, DK-2800, Lyngby, Denmark; and †Department of Chemistry, Building 207, Technical University of Denmark, DK-2800, Lyngby, Denmark

Received August 27, 1997; in revised form January 20, 1998; accepted January 27, 1998

Powder mixtures of metallic iron and sulfur have been milled in a high-energy planetary ball mill and the formation of iron sulfides has been studied by x-ray diffraction, Mössbauer spectroscopy, and scanning electron microscopy. For Fe : S ratios of 1 : 1 and 1 : 2 the final products are FeS with the modified NiAs structure and FeS_2 (pyrite), respectively. No other iron sulfides were formed for any of the Fe:S ratios studied. The FeS phase has been tested as an electrode material in lithium batteries.

Key Words: **mechanochemical reactions, iron sulfides, lithiation.**

1. INTRODUCTION

More than 20 years ago mechanical alloying was developed as a way to circumvent the limitations of conventional alloying, for example, for production of oxide dispersion-strengthened superalloys (1). Since the discovery of Koch *et al.* (2) demonstrating that amorphous $Nb_{40}Ni_{60}$ can be formed by mechanical alloying of elemental powder blends, mechanical alloying has emerged as a versatile technique for producing materials far from equilibrium in a variety of systems, for example, amorphous alloys, nanostructured alloys, and metastable solid solutions (3–6). In this metallurgical process, powder particles are subjected to severe mechanical deformation during collisions with balls and vial and are repeatedly deformed, cold welded, and fractured, so that solid-state reactions and/or mechanochemical reactions in powder blends can be generated. Although the principles governing these reactions in many cases are incompletely understood and are also undoubtedly system specific, the formation of many compounds prepared by mechanochemical reactions, for example, borides (7), carbides (8, 9), and silicides (10, 11), has been reported in the literature. However, relatively few studies of synthesis of metal sulfides have been published (12–21). On the other hand, sulfides are currently recognized as inorganic materials with interesting applications, for example, for high-energy density batteries, photoelectrolysis, solar energy materials, and precursors of superconductor syntheses, diagnostic and luminescence materials, and chalcogenide glasses (21). Although sulfides can be synthesised from the elements by heating (22), the degree of homogeneity of the final product may depend on preparation processes, starting materials, and the size of powders (23). This difficulty may be overcome by mechanical alloying in which coarse powders of different elements are milled together and form alloys by mechanochemical reactions.

In the present work, we describe in detail the phase evolution during mechanochemical reactions in the Fe–S system. The microstructural changes taking place were monitored by x-ray diffraction with Rietveld structure refinements, scanning electron microscopy (SEM), and Mössbauer spectroscopy. The magnetic structure of the milled FeS sample was investigated by low-temperature Mössbauer spectroscopy with and without applied magnetic fields. In addition, studies of electrochemical lithiation reactions of the milled FeS sample are presented.

2. EXPERIMENTAL

For the preparation powders of metallic iron (99.99% purity, particle size about 4 μm) and sulfur (99.9% purity, particle size about 50 μm, orthorhombic structure) were mixed in nominal compositions, 4 : 1, 1 : 1, 3 : 4, 1 : 2, and 1 : 3, and sealed in a vial in an argon atmosphere. The milling was carried out in a Fritsch Pulverisette 5 ball mill with tungsten carbide (WC) vials (75 mm in diameter, volume 250 ml) and balls (10 balls, 20 mm in diameter). The milling intensity was 200 rotations per minute and a ball-to-powder weight ratio of 20 : 1 was chosen. The milling process was interrupted after selected times to take out small amounts of powder for analysis.

The composition of the milled samples was examined using a Philips XL20 SEM with an energy dispersive x-ray analysis facility. To determine the surface oxidation of

[1]To whom correspondence should be addressed. E-mail: jiang@fysik.dtu.dk.

0022-4596/98 $25.00

milled particles, XPS measurements were carried out on a Perkin–Elmer 550 ESCA instrument in 10^{-7} Pa vacuum with an area of about 3×3 mm^2. X-ray diffraction measurements were performed using a Philips PW-3710 diffractometer with Cu$K\alpha$ radiation. The Rietveld refinement program (24) employed pseudo-Voigt functions limited to 9 half widths, asymmetry corrections, a mixing parameter $g = g_1 + g_2$ (2θ), ($g = 1$ for a pure Lorentzian and $g = 0$ for a pure Gaussian), and FWHM defined as $(U\tan^2\theta + V\tan\theta + W)^{1/2}$. g_1, g_2, U, V, and W are fitting parameters. Furthermore, the structure in the grain boundaries was assumed as an amorphous-like structure, which was modeled as a background by 15 parameters (Chebyshev type I) (24). Mössbauer spectroscopy was performed with a conventional constant acceleration spectrometer with a source of 50 mCi ^{57}Co in a Rh matrix. Isomer shifts are given relative to that of α-Fe at room temperature. A closed-cycle helium cryostat and a nitrogen cryostat were used for low-temperature Mössbauer measurements. One FeS sample milled for 113 h was tested at room temperature as electrodes in cathode limited lithium cells with organic electrolyte (1 M $LiPF_6$ in a 1 : 1 mixture of ethylene carbonate and diethyl carbonate). The cells were tested by constant current cycling between preset voltage levels (25).

3. RESULTS AND DISCUSSION

3.1. Alloying Process

All milled samples were investigated by x-ray diffraction. The x-ray diffraction patterns for the 0.5Fe–0.5S samples collected after different milling times as a typical example of the alloying process are shown in Fig. 1. After 1 h only diffraction lines due to α-Fe and S are seen. After 19 h weak diffraction lines corresponding to FeS and FeS_2 have already appeared. After 43 h the peaks due to α-Fe and S have almost disappeared and the peaks due to FeS are predominant. For longer milling times only the peaks due to FeS can be seen. These peaks are considerably broadened due to a small crystallite size and strain. Rietveld structural refinements of the whole x-ray diffraction patterns of the samples milled for 67, 90, and 113 h are shown in Fig. 2. It is found that the FeS phase formed in the milled samples has a modified NiAs-type structure with space group $P\bar{6}2c$. The lattice parameters and ionic positions are listed in Table 1. The analyses also revealed that both cationic and anionic vacancies are present in the milled FeS samples, although quantitative values of vacancy concentrations are subject to big uncertainties due to the broad diffraction lines. The Rietveld refinement analyses yield an accurate determination of diffraction line widths and positions. Attempts to use the simple NiAs symmetry ($P6_3/mmc$) resulted in slightly larger R factors. Using the formula derived by Stokes and Wilson (26) for diffraction line broadening, averaged crystallite sizes and root-mean-square (rms) strains of the FeS phase can be obtained in the milled samples, as listed also in Table 1. It is found that lattice parameter c of the FeS phase decreases with increasing milling time from 67 to 113 h, while parameter a remains nearly constant within experimental uncertainty. Lattice parameter c of the FeS phase in all samples is smaller than the data reported for bulk FeS phase (27). The average crystallite size of FeS decreases from 71 ± 5 nm (after 67 h) to 19 ± 5 nm (after 113 h), whereas the rms strain was slightly reduced from $1.6 \pm 0.1\%$ to $1.4 \pm 0.1\%$. The contraction along the c axis in the unit cell and the high values of rms strain may be linked to the presence of vacancies in the milled FeS phase.

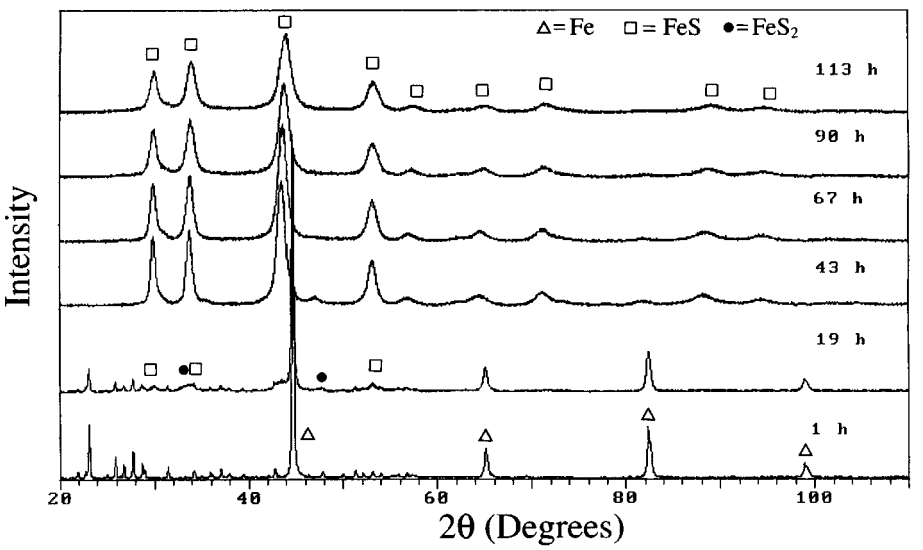

FIG. 1. X-ray powder diffraction patterns of the 0.5Fe–0.5S system for the samples collected after the indicated milling times.

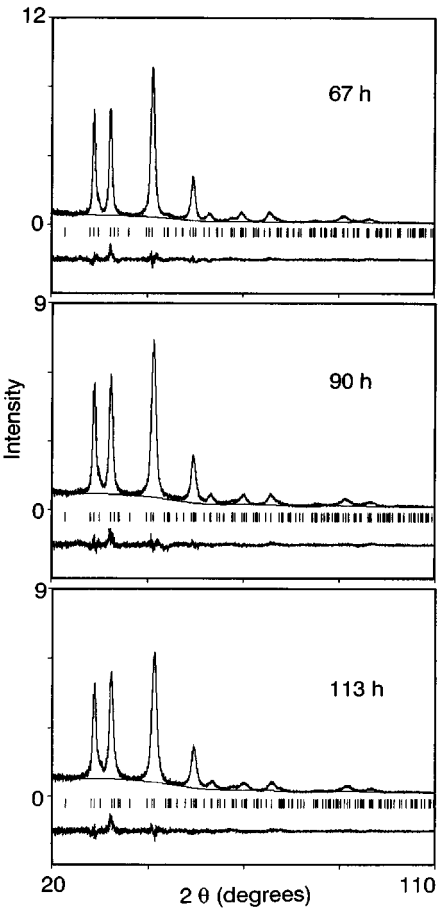

FIG. 2. Rietveld structure refinement profiles of the x-ray diffraction data for the 0.5Fe–0.5S samples milled for 67, 90, and 113 h. The experimentally observed pattern is shown in the upper field of each plot. Below that the background is also plotted as a solid line in this field. The difference pattern (observed minus calculated patterns) is plotted in the lower field. In the intermediate field the positions of the possible Bragg reflections are indicated as a series of short vertical bars corresponding to FeS crystalline phase with a modified NiAs-type structure in the samples.

Mössbauer spectra obtained at 295 and 80 K of the 0.5Fe–0.5S samples, collected after different milling times, are shown in Fig. 3. The data are in accordance with the results of x-ray diffraction. After 1 h only the sextet due to α-Fe is seen. After 19 h a quadrupole doublet with splitting $\Delta E_Q = 0.62 \pm 0.01$ mms^{-1} and isomer shift $\delta = 0.32 \pm 0.01$ mms^{-1} has appeared in the spectrum at 295 K. By comparison with the spectrum recorded at 80 K, it is found that the quadrupole splitting of the doublet does not depend on temperature. These results suggest that the doublet is attributed to low spin Fe^{2+} ions in pyrite (FeS_2) (28). The relative area of this doublet is about 12% at 295 K. Moreover, a new sextet with a relative area of about 14% at 295 K, magnetic hyperfine field, $B_{hf} \approx 27$ T, and isomer shift, $\delta \approx 0.7$ mms^{-1} has appeared. After 43 h this sextet has become predominant and only traces of the α-Fe and FeS_2 compounds can be seen. For longer milling times this sextet is the only component in the spectra at both 295 and 80 K. The lines of this sextet are relatively broad in all spectra, indicating a distribution in magnetic hyperfine fields. For simplicity, four sextets were used to fit the spectra at 295 K. The magnetic hyperfine fields for the first three sextets have a range of 25–30 T and the fourth sextet has a magnetic hyperfine field of about 20 T with very broad lines. In the spectra recorded at 80 K, the fourth sextet disappears, indicating that this sextet could be due to superparamagnetic relaxation effect. In most cases, superparamagnetic relaxation results in spectra composed of a sextet due to particles with relatively long relaxation times and a doublet (or singlet) due to particles with short relaxation times, but, if there is significant interparticle interaction one may instead observe spectra containing a sextet and a broad component (29). To identify the milled sample, we have compared the Mössbauer parameters with those of bulk FeS. The bulk FeS with the modified NiAs-type structure is antiferromagnetic with $T_N = 598$ K. At room temperature the Mössbauer parameters are $B_{hf} = 31.5$ T, $\delta = 0.76$ mms^{-1}, and the quadrupole shift is $\varepsilon = -0.19$ mms^{-1} (30). Cationic vacancies in the structure result in smaller magnetic hyperfine fields and isomer shifts. For example, the Mössbauer spectrum of ferrimagnetic Fe_7S_8, which also has a modified NiAs-type structure, can be fitted with five sextets with hyperfine fields ranging from 30.5 to 22.1 T and isomer shifts in the range 0.67–0.69 mms^{-1} (30). Thus, the low value of the average hyperfine field and the line broadening in the ball-milled samples may be explained by the presence of defects in the FeS structure, as observed in the Rietveld refinements. FeS can also have a tetragonal crystal structure, commonly called mackinawite (31). This phase does not show any magnetic ordering at temperatures as low as 1.7 K (31). A paramagnetic phase has also been found in high-pressure studies of FeS and Fe_7S_8 (30). In the present ball-milled samples we see, however, no indication of a paramagnetic phase after milling times exceeding 67 h. A preliminary study of mechanical alloying of a 0.5Fe–0.5S material in air was reported by Balaz *et al.* (17, 21). From x-ray diffraction measurements they suggested that $Fe_{1-x}S$ with a pyrrhotite 5C structure was formed in the milled sample, in which sulfate and iron oxide layers were found on surfaces of milled powders. In fact, there are many sulfide compounds with slightly different structures around the 0.5Fe–0.5S composition (32). It could be indeed difficult to distinguish them by x-ray diffraction measurements alone. Therefore, in-field and low-temperature Mössbauer measurements of the as-milled FeS sample were performed. A broadened sextet was observed down to 14 K for the FeS sample. No iron oxide phases were found. Application of a magnetic field of 0.7 T perpendicular to the gamma ray direction at 300 and 80 K has negligible influence on the

TABLE 1
Lattice Parameters, Ionic Positions, Reliability *R* Factors, Average Crystallite Sizes, and Strains of the FeS Phase in the 0.5Fe–0.5S Samples after Milling Times of 67, 90, and 113 h

Milling time (h)	*a* (Å)	*c* (Å)	Ion	*x*	*y*	*z*	*R* (%)[a]	Crystallite size (nm)	Strain (%)
67	5.961(3)	11.519(2)	Fe	0.343(1)	− 0.011(1)	0.125(2)	4.76	72(5)	1.6(1)
			S1	0.000	0.000	0.000			
			S2	1/3	2/3	− 0.018(1)			
			S3	0.664(2)	0.001(2)	0.250			
90	5.965(3)	11.448(2)	Fe	0.342(2)	− 0.007(2)	0.122(1)	5.43	31(5)	1.5(1)
			S1	0.000	0.000	0.000			
			S2	1/3	2/3	− 0.019(1)			
			S3	0.660(3)	0.009(4)	0.250			
113	5.964(2)	11.399(2)	Fe	0.357(3)	− 0.005(1)	0.129(1)	5.56	19(5)	1.4(1)
			S1	0.000	0.000	0.000			
			S2	1/3	2/3	− 0.018(1)			
			S3	0.678(3)	− 0.021(2)	0.250			
FeS (Ref. 27)	5.963(1)	11.754(1)	Fe	0.3787(2)	0.0553(2)	0.1230(9)	—	—	—
			S1	0.0000	0.0000	0.0000			
			S2	1/3	2/3	0.0208(2)			
			S3	0.6648(6)	− 0.0041(4)	0.2500			

Note. These data are obtained by the Rietveld structure refinements. Data from bulk FeS are also included (27).
[a] $R = \sum |y_{\mathrm{obs},i} - y_{\mathrm{cal},i}| / \sum y_{\mathrm{obs},i}$, where $y_{\mathrm{obs},i}$ and $y_{\mathrm{cal},i}$ represent the observed and calculated intensities at the ith step, respectively.

spectrum of FeS sample, as shown in Fig. 4. However, pyrrhotite $Fe_{1-x}S$ phases are ferrimagnetic and FeS is antiferromagnetic (33). For a ferro- and ferri-magnetic material the relative intensities of lines of 2 and 5 would increase. By combining x-ray diffraction with in-field Mössbauer measurements, we suggest that the phase formed in the final stage of milling in the present work is antiferromagnetic FeS with a modified NiAs-type structure containing both cationic and anionic vacancies. It is, however, possible that the spin structure to some extent could be canted due to defects formed during the ball milling process.

X-ray diffraction and Mössbauer spectroscopy measurements on other compositions with various milling times have also been performed. It was found that for the 0.33Fe–0.67S composition the formation process of FeS_2 (pyrite) is much slower than that of FeS in the 0.5Fe–0.5S composition. The FeS_2 phase was synthesised with prolonged times ($\geq$110 h). Low-temperature Mössbauer measurements of the as-milled FeS_2 sample were performed. Only a doublet was observed down to 14 K. No iron oxide phases were found. For other compositions, instead of single phase, mixtures of phases were observed in the final milling stages ($\geq$110 h). The details of the kinetic processes of phase transformation for all compositions are given later.

SEM was employed to monitor microstructural evolution in the powder blends during the milling process. SEM micrographs of Fe–S mixtures after various milling times are shown in Figs. 5–8. Using a backscattered electron detector, signals from heavy atoms are enhanced compared to those from light elements. Energy dispersive x-ray analysis (EDX) provides further information about the chemical composition of the milled powders. As shown in Fig. 5a for the 0.5Fe–0.5S composition, the iron particle morphology, after a milling time of 1 h, is similar to that of the starting materials, consisting of spherical-like particles with a size distribution. In the backscattered electron image (Fig. 5b) on the same spot a relatively broad dispersion of particle sizes is visible. This could be due to the signal depression from coated sulfur layers on iron particles. In general, during the milling process the local temperature at collisions with balls and vial is assumed to be higher than 373 K (34), although the vial temperature is found to be about 332 K after ball milling in the present work. Hence, in the Fe–S system, sulfur could be melted in the initial milling process because its melting temperature is only 390 K. Figure 5c shows sulfur-coated iron particles at high magnification. It is clearly seen that the cloudy sulfur wet a deformed iron particle. Assuming that all sulfur in the 0.5Fe–0.5S sample coated iron particles with a size of 3 μm, a sulfur layer can be estimated to be about 750 nm. Moreover, EDX results of the sample milled for 1 h in many places with an area of about $0.2 \times 0.2\ \mathrm{mm}^2$ reveal a strong signal from iron and very weak signal from sulfur. This might be explained by the thin sulfur layer on spherical-like iron particles because the detector receives most of EDX signals from a pear-shaped zone beneath sulfur layer down to about 3 μm using an electron beam energy of 20 kV. Thus, the signal from iron is dominant in EDX measurements. On grinding for 19 h,

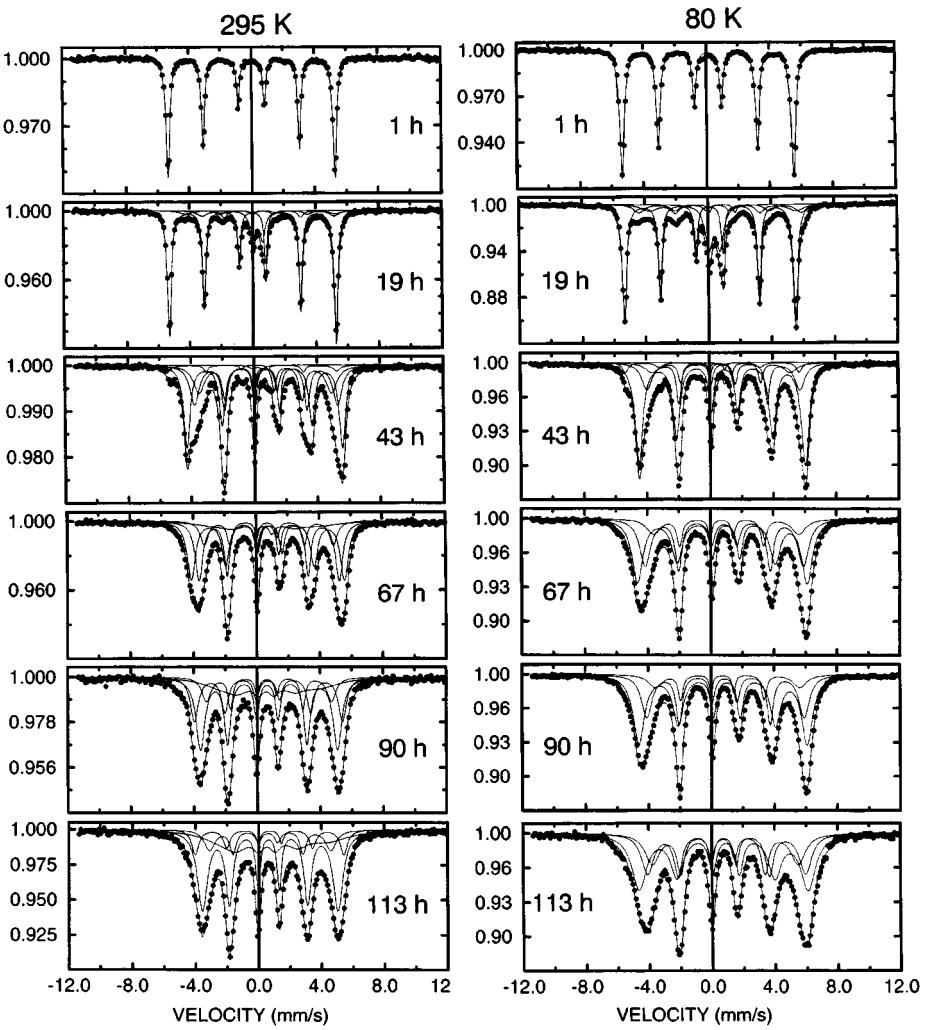

FIG. 3. Mössbauer spectra obtained at 295 and 80 K of the 0.5Fe–0.5S samples collected after the indicated milling times.

spherical-like particles were plastically deformed into disk-like pellets (Figs. 6a and 6b). Relatively larger signals from sulfur were detected by EDX. This has presumably resulted from the formation of Fe–S compounds at interfaces between the iron pellets and the sulfur layer and/or more sulfur-coated areas exposed to electron beams. After 43 h, the sample consists of two distinct parts (Fig. 7a). One part is composed of very small fragments with more or less equiaxial particles with sizes less than 1 μm (Fig. 7d) and the other part is composed of larger agglomerates which are larger than the starting iron powders, as shown in Figs. 7a–7c. Most of these particles are dense. However, porous fine particles (Figs. 7b and 7c), resembling a partially sintered material, were also found. EDX measurements showed that both fine and big particles have a composition of about Fe:S = 1:1. A similar particle morphology was also reported in other *M*–S (M: metal elements) systems (14–17), in which the formation of big particles was suggested due to self-sustaining reactions during grinding (35). However, from x-ray diffraction and Mössbauer measurements, it was found that most of the mechanochemical reactions in the 0.5Fe–0.5S powder blends have already been finished after 43 h milling. If these clumps were formed by self-sustaining reactions within milling times ranging from 19 to 43 h, then it is expected that most of the clumps should be broken into small fragments during further milling. This explanation is challenged by the fact that many clumps were still observed in the samples milled for 67, 90, and 113 h (Fig. 8). Apart from the possibility of self-sustaining reactions, we suggest that these big agglomerates are most likely generated by powder pressing and sintering. It was observed that the balls and the wall of the vial were nearly covered by powders.

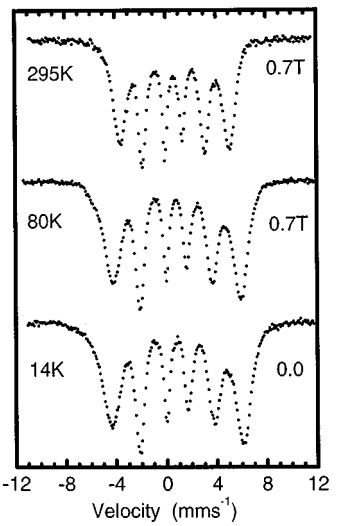

FIG. 4. Mössbauer spectra of the as-milled FeS sample obtained at 295 and 80 K with an applied magnetic field of 0.7 T and at 14 K.

When collisions with balls and wall occur, the powders in between will be pressed and sintered. This process could form relatively dense clumps, as observed in Fig. 8.

The kinetic process of phase evolution during mechanical alloying of elemental blends for three compositions, 0.5Fe–0.5S, 0.43Fe–0.57S, and 0.33Fe–0.67S, is shown in Fig. 9. The data were determined from room-temperature Mössbauer measurements assuming equal recoil-free factors for all phases. Note that pure sulfur cannot be detected by Mössbauer spectroscopy and is hardly detectable by x-ray diffraction due to low atomic weight. In the milling process, several reactions could take place and they are probably dynamic processes. For simplicity, only four chemical reactions were used to analyze the mechanochemical reaction process in the Fe–S system. They are (a) $Fe + S = FeS$ with a negative free energy of formation at 295 K, $\Delta G \approx -24$ kcal/mol; (b) $Fe + 2S = FeS_2$ with $\Delta G \approx -40$ kcal/mol; (c) $FeS + S = FeS_2$ with $\Delta G \approx -16$ kcal/mol; and (d) $FeS_2 + Fe = 2FeS$ with $\Delta G \approx -8$ kcal/mol (36). In the early stage, FeS is formed together with FeS_2 on grinding elemental powder mixture in all systems studied, although FeS has a smaller negative free energy of formation than FeS_2 (25). This indicates that reactions (a) and (b) could govern the mechanochemical reactions in the early milling stages. By further increasing the milling time, the process (d) occurs in the 0.5Fe–0.5S sample, which accelerates the formation of the FeS phase in the sample. After 43 h, 96% of the total amount of iron is found in the FeS phase and only FeS was observed in the samples milled for ≥ 67 h. In the case of Fe:S = 1:2, the relative amounts of both FeS and FeS_2 phases increase from

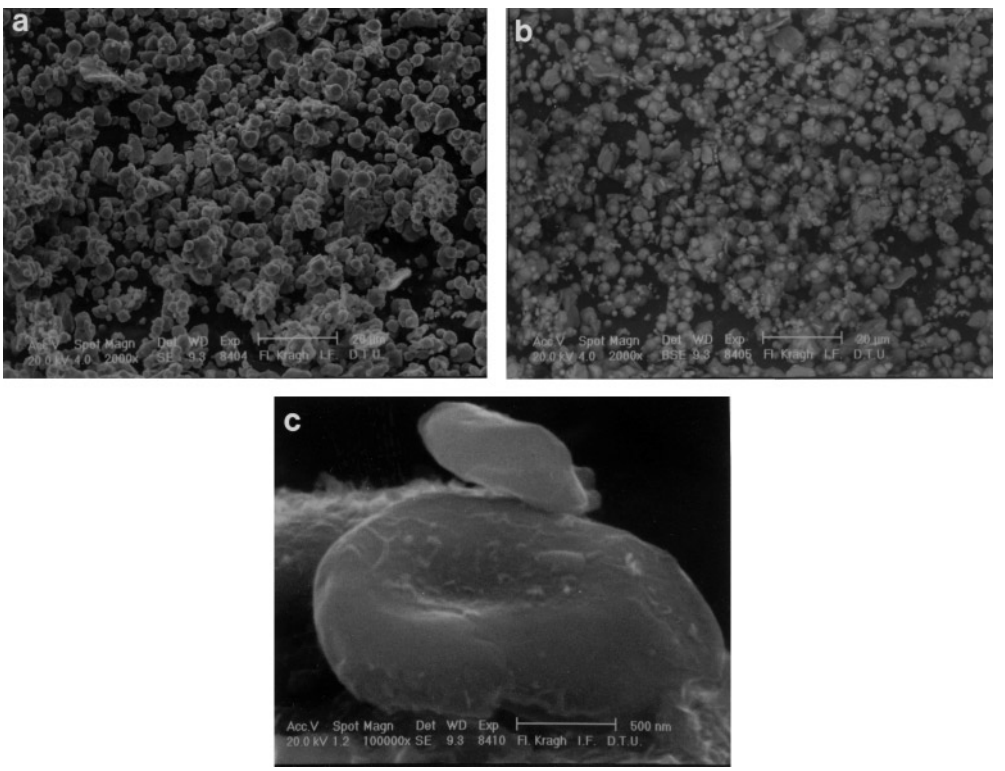

FIG. 5. SEM micrographs of the 0.5Fe–0.5S sample milled for 1 h: (a) and (c) using secondary electron detector and (b) using backscaterred electron detector.

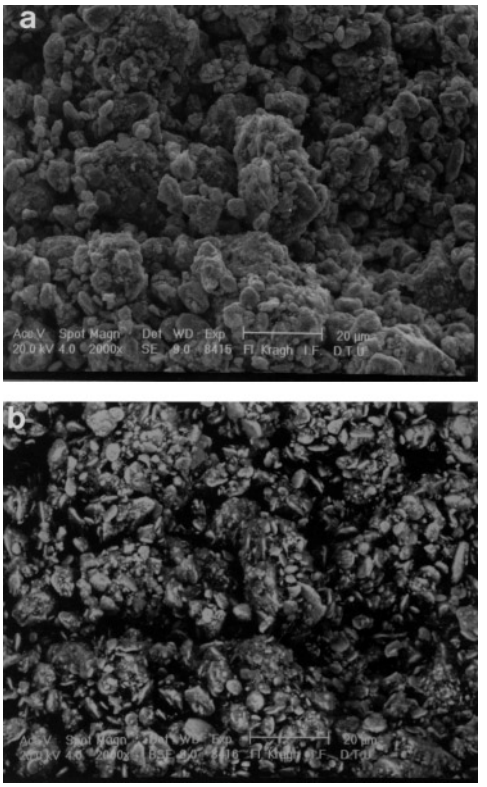

FIG. 6. SEM micrographs of the 0.5Fe–0.5S sample milled for 19 h: (a) using secondary electron detector and (b) using backscaterred electron detector.

19 to 42 h. Then, it almost saturates for the FeS phase while the fraction of the FeS_2 phase still increases, indicating that reaction (b) governs the mechanochemical reactions during grinding. After 67 h, the amount of FeS_2 increases at the expense of FeS phase. This infers that reaction (c) occurs. Within experimental uncertainty only the FeS_2 phase was observed in the sample milled for 110 h. For the $Fe:S = 3:4$ composition, the mechanochemical reaction process looks quite similar to that in the 0.33Fe–0.67S sample until 43 h. With further grinding, reaction (a) prevails during further milling while no more residual sulfur provides for reactions (b) and (c). After 67 h, the system reaches an equilibrium state, in which the relative fractions of FeS and FeS_2 remain nearly unchanged. It is possible that the recoil-free factors for both phases could be slightly different at room temperature. This may explain why only about 61% of FeS, instead of 67%, was found in the final stage of the sample. No formation of Fe_3S_4 was found in the study. If one looks at the relative fraction of iron vs milling time in various compositions, one striking feature can be drawn: the more iron in the sample, the faster the mechanochemical reactions. For example, even after 110 h milling, *bcc*-Fe was still found in the composition of $Fe:S = 1:3$. On the other hand, FeS and FeS_2 phases have already been found in the 0.8Fe–0.2S sample milled only for 1 h. The relative fractions of *bcc*-Fe (about 73%), FeS (about 23%), and FeS_2 (about 4%) phases in 0.8Fe–0.2S samples remain almost unchanged after 19 h.

Room-temperature Mössbauer spectra for the as-milled Fe–S samples with various compositions after a milling time of about 110 h are shown in Fig. 10. Table 2 provides a list of crystalline phases with relative molar fractions obtained by room-temperature Mössbauer spectroscopy measurements assuming equal recoil-free factors for all phases, for milled elemental blends in various compositions after a milling time of about 110 h. In the 0.5Fe–0.5S composition nanostructured FeS materials are formed after a milling time of about 67 h with very low abrasive wear contamination (less than 0.5 at.% W), details given later. In the 0.33Fe–0.67S composition, the FeS_2 phase is also achieved on grinding with prolonged times (≥ 110 h). The decomposition process of FeS_2 into FeS and S, which is unfavored from the free energy of formation of FeS_2, was not observed in the study, but the decomposition was reported by Avvakumov and Kosobudjkij (12). In their study the local temperature at collisions might be so high that the decomposition of FeS_2 into FeS and S is energetically favored. In the case of $Fe:S = 3:4$, after prolonged milling times (up to 150 h), only a mixture of FeS and FeS_2 phases was obtained and no Fe_3S_4 phase was formed. This could be due to the fact that Fe_3S_4 is a metastable phase compared to FeS and FeS_2 phases. A mixture of *bcc*-Fe, FeS, and FeS_2 phases was observed in both $Fe:S = 4:1$ and $Fe:S = 1:3$ compositions. No Fe–S solid solutions were found in the 0.8Fe–0.2S sample milled for 110 h within experimental uncertainty, as predicted by the equilibrium Fe–S phase diagram indicating a negligible solubility of sulfur in *bcc*-Fe at temperatures below 1173 K (37). No other new Fe–S phases were formed during mechanical alloying of elemental blends.

3.2. *Characterization of the Milled Samples*

Compared to milling of oxides and some hard metals, abrasive wear of balls and vial is negligible in the Fe–S system. The very small contamination of the milled products by W presumably indicates that the hardness of Fe–S compounds formed during milling may remain less than ball hardness. It was also observed that the surface of the balls and the interior wall of the vial were covered by powders, so that less abrasive wear of balls and vial is expected. Furthermore, no contamination in the milled powders infers that chemical affinity between powders and the milling tungsten carbide balls and vial is weak. This is indeed experimentally indicated by Kosmac and Courtney (14) that no chemical reaction occurs between W and S elemental powders during high energy ball milling. They suggested that a high melting point of W compared to Ni, Zn, Sn, and Fe could be a plausible reason for the effect, although the heat of phase formation of the respective metal sulfides do not differ all that much (38). However, it is

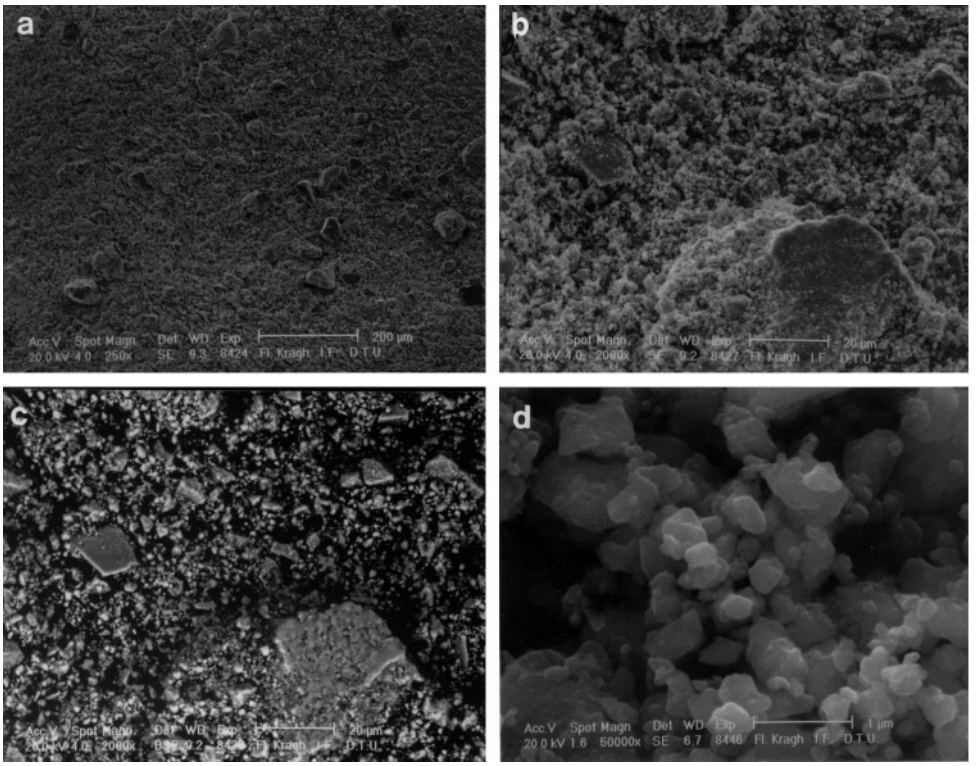

FIG. 7. SEM micrographs of the 0.5Fe–0.5S sample milled for 43 h: (a), (b), and (d) using secondary electron detector and (c) using backscaterred electron detector.

known that WS_2 has a weakly bonded layer structure, which has the same space group ($P6_3/mmc$) as graphite. The WS_2 material could act as a lubricant media during grinding. Thus the shear effect induced during collisions, which is an important factor for mechanical alloying in many cases, could be largely reduced. No further reaction between W and S can occur. To test the validity of this model, a milling experiment of elemental Mo and S blends using the same setup as in the Fe–S system was carried out because MoS_2 also has a weakly bonded layer structure (39). It was indeed found that almost no chemical reaction between Mo and S after a milling time of 110 h was observed, as is the case in the W and S system. By careful examination of the x-ray diffraction pattern of the sample milled for 110 h, as shown in Fig. 11, a small amount of MoS_2 can be detected, although the pattern mainly consists of pure Mo and S phases. In addition, the diffusion coefficients of sulfur in WS_2 and MoS_2 are about four orders magnitude smaller than those in FeS and NiS (40). This means that fresh sulfur may have low possibilities to diffuse through the MoS_2 layer formed between sulfur and molybdenum to react further with molybdenum. Hence, this tiny MoS_2 phase might be the key factor for no further reaction between Mo and S during prolonged milling.

To further characterize the iron sulfides, the oxidation of powdered samples on exposure to air at ambient temperature was examined by XPS and Mössbauer spectroscopy. XPS spectra of S(2p) electrons from the as-milled FeS sample (milled for 113 h) and the samples after *in situ* sputtering treatments for 25, 85, and 1500 s are shown in Fig. 12. It is found that the state of sulfur on the surface of FeS powders is composed of dominant line of S^{2-} and a small component of sulfate SO_4^{2-}. It is interesting to know how deep the sulfur in the milled FeS powders was oxidized. After about 3 monolayers are removed by *in situ* ion beam sputtering for 25 s, the spectrum shows only the S^{2-} line and no sulfate line within experimental uncertainty. The XPS spectra after sputtering for longer times show only the S^{2-} line. When the FeS powders are exposed to air after a milling time of 113 h, a few monolayers of the powders are oxidized. This passivation layer retards further oxidation of the powders, which was confirmed by XPS measurements from the sample kept in air at ambient temperature for about 30 days. In addition, no difference was observed by Mössbauer measurements for the as-milled FeS sample and the sample after exposure to air for about 30 days. These results revealed that the as-milled FeS powders studied are relatively pure as compared with the sample prepared by

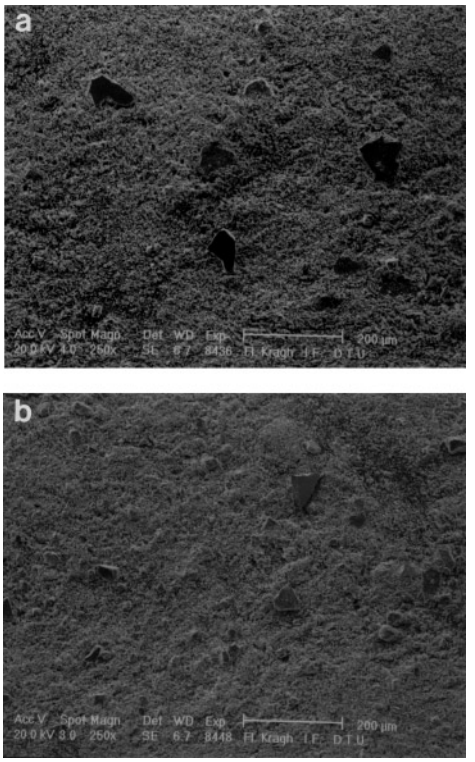

FIG. 8. SEM micrographs of the 0.5Fe–0.5S samples obtained by secondary electron detector milled for (a) 67 h and (b) 113 h.

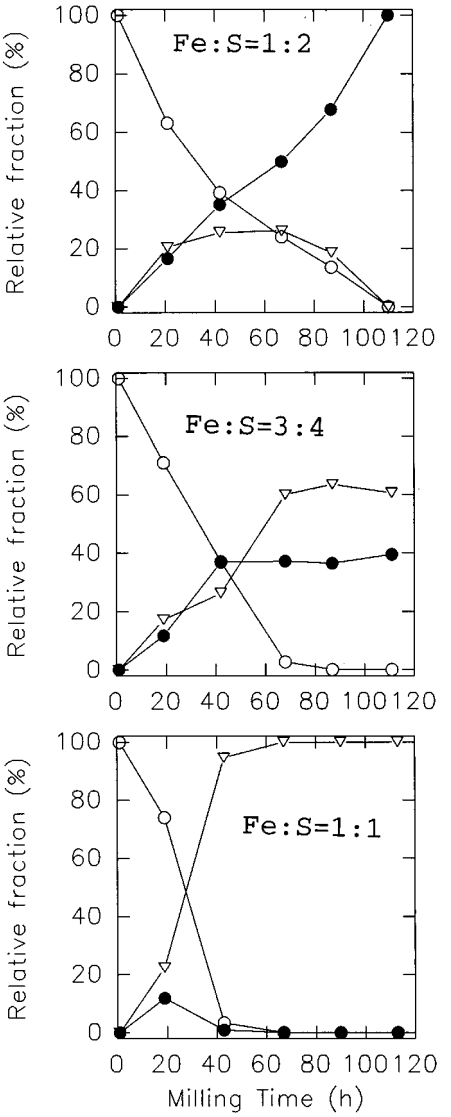

FIG. 9. Relative fractions of various phases during mechanical alloying of elemental Fe–S blends for three compositions as a function of milling time. The empty circles represent *bcc*-Fe, the full circles represent FeS_2, and the triangles indicate FeS.

Balaz *et al.* (17). They prepared FeS powders by mechanochemical synthesis *in air* from elemental Fe and S powders, in which the sulfate SO_4^{2-}, was found to be dominant.

In the case of FeS_2, the oxidation process is much faster when the powders are exposed to air. Besides the surface oxidation, the interior of the milled FeS_2 powders is partially oxidized. Room-temperature transmission Mössbauer spectra for the as-milled sample and the sample exposed to air for about 30 days at ambient temperature are shown in Fig. 13. By comparison with the as-milled sample, the spectrum for the sample exposed to air for about 30 days has two doublets, one is due to FeS_2 having a quadupole splitting of about 0.61 ± 0.01 mm/s and an isomer shift of 0.31 ± 0.01 mm/s, and the other has a quadrupole splitting of about 2.53 ± 0.01 mm/s and an isomer shift of 1.33 ± 0.01 mm/s with a relative area of about 24%. The latter is attributed to an iron sulfate (28), $FeSO_4$ (H_2O cannot be ruled out), which is also formed during surface oxidation of bulk FeS_2 in air (41). It is clear that the milled FeS_2 powders are unstable in air, in distinction to the relatively stable milled FeS powders. Wang *et al.* (42) demonstrated that when FeS_2 surfaces are in contact with water and oxygen, the oxidation process occurs rapidly. Furthermore, small

TABLE 2

Crystalline Phases with Relative Molar Fractions as Detected by Room-Temperature Mössbauer Spectroscopy Measurements Assuming Equal Recoil-Free Factors for All Phases in Various Compositions after a Milling Time of about 110 h

Fe:S composition	*bcc*-Fe (%)	FeS (%)	FeS_2 (%)
4:1	73	23	4
1:1	—	100	—
3:4	—	61	39
1:2	—	—	100
1:3	21	25	54

Note. The uncertainties of relative molar fractions for various phases are about 3%.

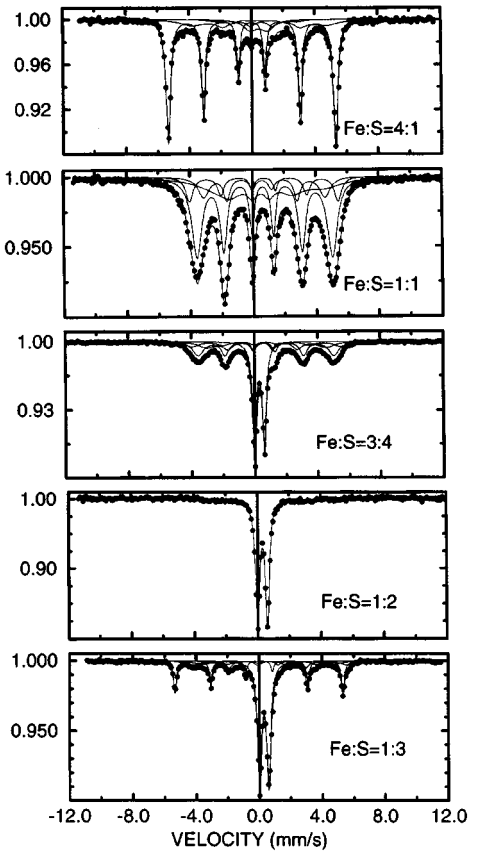

FIG. 10. Room-temperature Mössbauer spectra for the as-milled Fe–S samples after a milling time of about 110 h with various compositions.

particle sizes and defects in the milled FeS_2 may also enhance the oxidation process. If the oxidation processes for the milled FeS and FeS_2 powders are assumed to be $FeS + 2O_2 = FeSO_4$ and $FeS_2 + 3O_2 = FeSO_4 + SO_2$, respectively, one can find that the exothermic heat released by

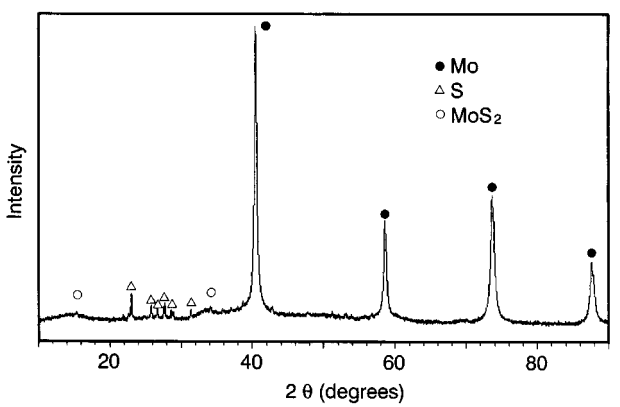

FIG. 11. The x-ray diffraction pattern of the 0.33Mo–0.67S sample milled for 110 h.

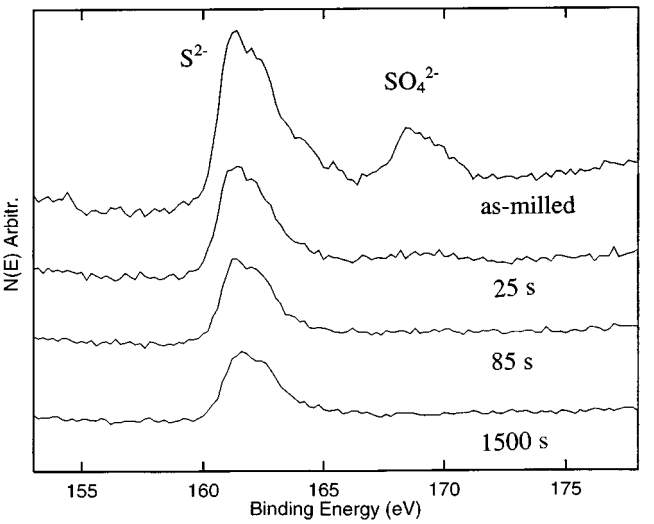

FIG. 12. S(2*p*) photoelectron spectra for the as-milled FeS sample and the samples *in situ* sputtered for 25, 85, and 1500 s.

the oxidation process of FeS_2 is lager than that of FeS (36). This may accelerate the oxidation process in the milled FeS_2 powder. To clarify the difference of oxidation processes in both FeS and FeS_2 samples, however, further studies are needed.

3.3. *Electrochemical Lithiation Reactions*

One application of iron sulfides is as active electrode materials for primary lithium batteries of high energy density. During discharge of these cells, iron sulfide is reduced to a mixture of metallic iron and lithium sulfide according to the reaction schemes

$$2Li + FeS \rightarrow Li_2S + Fe$$

$$4Li + FeS_2 \rightarrow 2Li_2S + Fe,$$

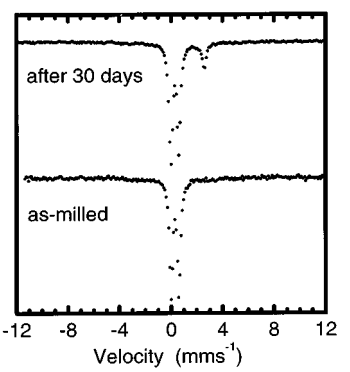

FIG. 13. Room-temperature Mössbauer spectra of the as-milled FeS_2 sample and the sample exposure to air at ambient temperature for about 30 days.

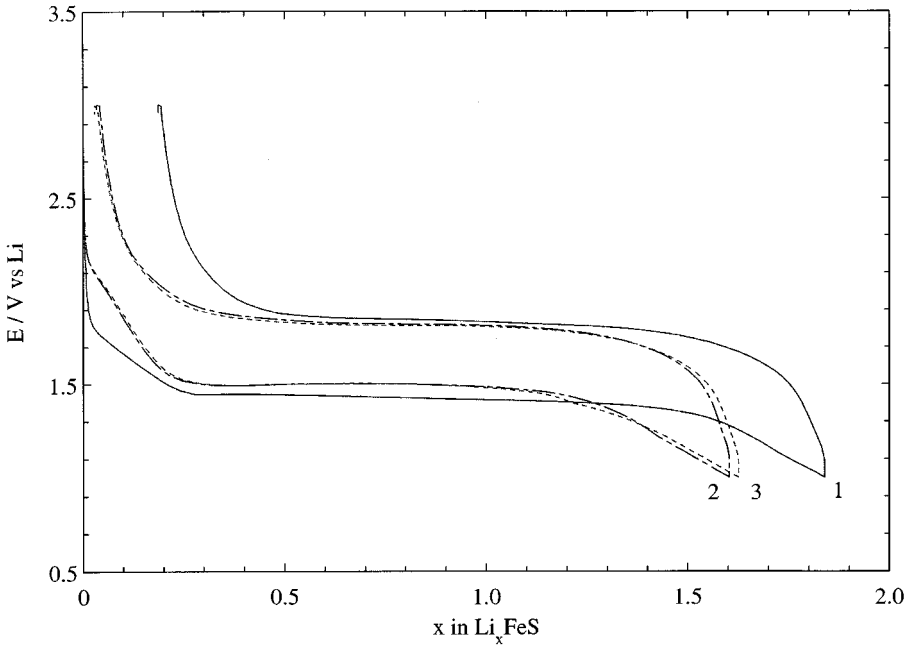

FIG. 14. Voltage of a Li/organic electrolyte/FeS cell as function of the degree of lithiation of the iron monosulfide prepared by mechanochemical reaction of 0.5Fe–0.5S elemental blends. Data for the first three cycles (indicated on the graph) are shown. Current density $\sim 200\ \mu A/cm^2$, corresponding to 24 h discharge.

where a defect iron sulfide, $Fe_{1-x}S$, is formed as an intermediate in the reduction of the disulfide (25). In the case of the monosulfide, the lithiation reaction can be reversed a number of times due to the intimate mixture and good conductivity of the reaction products. This makes iron monosulfide a candidate electrode material for secondary (rechargeable) lithium batteries for applications where high energy density is more important than long cycle life.

It has previously been shown (see (25) and references therein) that the voltage profile of lithium/iron sulfide cells is sensitive to the structural composition of the iron sulfide. Free elemental sulfur will react with lithium at a voltage significantly higher than the reaction with either iron monosulfide or disulfide. A significant difference is also observed between the initial discharge curves of cells made with iron monosulfide with the modified NiAs-type structure compared to the Mackinawite, FeS, with a tetragonal structure. The latter shows an initial discharge plateau at 1.8 V after which the voltage drops to 1.5 V, whereas the NiAs modification discharges in a single plateau close to 1.5 V. Figure 14 shows the first three lithiation/extraction (discharge/charge) cycles of a cell with FeS milled for 113 h. It is seen that the initial discharge proceeds in a single step at 1.5 V with a capacity close to the expected 2 Li per Fe. Capacity plateaus at 2.5 V characteristic of unreacted elemental sulfur or at 1.8 V characteristic of the Mackinawite phase are not observed. Initially, the capacity drops after the first cycle, but then stays nearly constant in the subsequent five cycles. The electrochemical measurements are in accordance with the fact that the milled product is FeS with the modified NiAs-type structure, with no electrochemically active impurities. The material prepared by ball milling is well suited for the use as electrode material, giving a high utilization and good cycling performance.

4. CONCLUSIONS

It has been shown that ball-milling of elemental powders of iron and sulfur can be applied to produce iron sulfides. For Fe:S ratios of 1:1 and 1:2, the final products are FeS with the modified NiAs structure and FeS_2 (pyrite), respectively. The FeS phase contains both cationic and anionic vacancies. For other Fe:S ratios we observe the same two phases together with *bcc*-Fe (for $Fe:S = 4:1$) and S (for $Fe:S = 1:3$). No indication of the spinel Fe_3S_4 was observed. The FeS_2 phase reacts with ambient air and forms iron sulfate, whereas only a few surface layers of sulfate are formed on the FeS particles. The FeS phase is well suited as an electrode material in lithium batteries.

ACKNOWLEDGMENTS

This work was financially supported by the Danish Technical Research Council. Particular thanks go to A. Schøneberg and L. L. Berring for their assistance in x-ray diffraction measurements, to F. Kragh for his assistance in SEM measurements and to J. Larsen for his assistance in XPS measurements.

REFERENCES

1. J. S. Benjamin, *Metall. Trans.* **1,** 2943 (1970).
2. C. C. Koch, O. B. Cavin, C. G. McKamey, and J. O. Scarbrough, *Appl. Phys. Lett.* **43,** 1017 (1983).
3. W. L. Johnson, *Prog. Mater. Sci.* **30,** 81 (1986).
4. C. C. Koch, *in* "Materials Science and Technology" (R. W. Cahn, P. Haasen, and E. J. Kramer, Eds.), Vol. 15, p. 193. VCH Weiheim, Germany, 1991.
5. R. Bormann, International conference on Materials by Powder Technology, Dresden, Germany, Mar. 23–26, 1993, DGM Informationsgesellschaft Verlag, Germany, 1993, p. 247; and J. Z. Jiang, C. Gente, and R. Bormann, *Mater. Sci. Eng. A* **242,** 268 (1998).
6. J. Z. Jiang, R. Lin, S. Mørup, K. Nielsen, F. W. Poulsen, F. J. Berry, and R. Clasen, *Phys. Rev. B* **55,** 11 (1997); and J. Z. Jiang, S. Mørup, and S. Linderoth, *Mater. Sci. Forum* **225–227,** 489 (1996).
7. L. Schultz, J. Wecker, and E. Hellstern, *J. Appl. Phys.* **61,** 3583 (1987).
8. P. Matteazzi and G. Le Caër, *J. Am. Ceram. Soc.* **74,** 1382 (1991).
9. G. Le Caër, E. Bauer-Grosse, A. Pianelli, E. Bouzy, and P. Matteazzi, *J. Mater. Sci.* **25,** 4726 (1990).
10. R. K. Viswanadham, S. K. Mannan, and S. Kumar, *Scr. Metall.* **22,** 1011 (1988).
11. C. G. Tschakarov, V. Rusanov, and G. Gospodinov, *J. Solid State Chem.* **59,** 265 (1985).
12. E. G. Avvakumov and I. D. Kosobudjkij, *Izv. Sib. Otd. Acad. Nauk SSSR* **5,** 135 (1973).
13. V. Rusanov and C. Chakurov, *J. Solid State Chem.* **79,** 181 (1989).
14. T. Kosmac and T. H. Courtney, *J. Mater. Res.* **7,** 1519 (1992).
15. T. Kosmac, D. Mauric, and T. H. Courtney, *J. Am. Ceram. Soc.* **76,** 2345 (1993).
16. P. Balaz, T. Havlik, J. Briancin, and R. Kammel, *Scr. Metall. Mater.* **32,** 1357 (1995).
17. P. Balaz, T. Havlik, Z. Bastl, and J. Briancin, *J. Mater. Sci. Lett.* **14,** 344 (1995).
18. T. Ohtani, M. Motoki, K. Koh, and K. Ohshima, *Mater. Res. Bull.* **30,** 1495 (1995).
19. L. Takacs, *Appl. Phys. Lett.* **69,** 436 (1996).
20. L. Takacs and M. A. Susol, *J. Solid State Chem.* **121,** 394 (1996).
21. P. Balaz, Z. Bastl, T. Havlik, J. Lipka, and I. Toth, *Mater. Sci. Forum* **235–238,** 217 (1997).
22. F. Jelinek, *in* "MTP International Review of Science Inorganic Chemistry," Series I, Vol. 5, p. 339. Butterworth, London, 1972.
23. I. J. Lin and S. Nadiv, *Mater. Sci. Eng.* **39,** 193 (1979); and P. Toulmin and P. B. Barton, *Geochim. Cosmochim. Acta* **28,** 641 (1964).
24. J. Z. Jiang, R. Lin, K. Nielsen, S. Mørup, D. G. Rickerby, and R. Clasen, *Phys. Rev. B* **55,** 14830 (1997).
25. K. Hansen and K. West, Proceedings of The Electrochemical Society 1997 Joint International Meeting, Sept. 1997, Paris, in press.
26. A. R. Stokes and A. J. C. Wilson, *Proc. Phys. Soc.* **56,** 144 (1944).
27. H. E. King and C. T. Prewitt, *Acta Crystallogr. B* **38,** 1877 (1982).
28. N. N. Greenwood and T. C. Gibb, "Mössbauer Spectroscopy." Chapman and Hall, London, 1971.
29. S. Mørup, F. Bødker, P. V. Hendriksen, and S. Linderoth, *Phys. Rev. B* **52,** 287 (1995).
30. H. Kobayashi, M. Sato, T. Kamimura, M. Sakai, H. Onodera, N. Kuroda, and Y. Yamagguchi, *J. Phys. C* **9,** 515 (1997).
31. E. F. Bertant, P. Burlet, and J. Chappert, *Solid State Commun.* **3,** 335 (1965).
32. For example, see JCPDS cards: 11-151, 20-534, 22-1120, 24-79, 24-80, 24-220, 25-411, 29-726, 29-723, 29-724, 29-725, and 37-477, Published by the International Centre for Diffraction Data, 1601 Park Lane, Swarthmore, PA 19081.
33. L. M. Levinson and D. Treves, *J. Phys. Chem. Solids* **29,** 2227 (1968).
34. J. S. Benjamin, *Mater. Sci. Forum* **88–90,** 1 (1992); and R. M. Davis, B. McDermott, and C. C. Koch, *Metall. Trans. A* **19,** 2867 (1988).
35. J.-P. Lebrat, A. Varma, and A. E. Miller, *Metall. Trans. A* **23A,** 69 (1992).
36. R. C. Weast, M. J. Astle, and W. H. Beyer, "CRC Handbook of Chemistry and Physics," p. D-71. CRC Press, Boca Raton, FL, 1985; and T. Rosenqvist, "Principles of Extractive Metallurgy," p. 521. McGraw–Hill, New York, 1974.
37. Metals Handbook, "Metallography, Structures and Phase Diagrams," Vol. 8, p. 305. American Society for Metals, Metals Park, OH, 1973.
38. W. N. Tuller, "The Sulphur Data Book," McGraw–Hill, New York, 1954.
39. J. V. Smith, "Geometrical and Structural Crystallography," p. 313. Wiley, New York, 1982.
40. S. Mrowec, *React. Solids* **5,** 241 (1988).
41. A. N. Buckley and R. Woods, *Appl. Surface Sci.* **27,** 437 (1987).
42. X. H. Wang, C. L. Jiang, A. M. Raichur, R. K. Parekh, and J. W. Leonard, *Proc. Electrochem. Soc.* **17,** 410 (1992).